

Article

# Waste-to-Reuse Foam Glasses Produced from Soda-Lime-Silicate Glass, Cathode Ray Tube Glass, and Aluminium Dross

Meriem Sassi and Andrea Simon \* 

Institute of Ceramics and Polymer Engineering, University of Miskolc, 3515 Miskolc-Egyetemvaros, Hungary; sassi90meriem@gmail.com

\* Correspondence: simon.andrea@uni-miskolc.hu

**Abstract:** Aluminium dross is a hazardous industrial waste generated during aluminium production. It contains metallic oxides of aluminium and magnesium, other phases (aluminum nitride), and residues of fluxes and salts from the melting process of aluminium. Discarding this by-product is considered an environmental and economic challenge due to the high reactivity of dross with water or even air humidity. After removing the hazardous components from the as-received dross, one of the optional approaches is to incorporate the treated dross into construction materials. Dross is applied in several types of research as a secondary raw material source for alumina, clinker, cement or glass-ceramic production, but only a few papers focus on the usage of dross as a foaming agent for foams. Even fewer research are reported where dross was applied as a basic component of foam glasses. In this work, foam glasses were produced completely from waste materials: Aluminium dross, container (SLS) glass, and cathode ray tube (CRT) glass. The research holds several specificities, i.e., combining two industrial waste materials (CRT glass and dross), and adding an increased amount from the wastes. The physical and mechanical characteristics were examined with a special focus on the effect of the foam glass components on the microstructure, density, thermal conductivity, and compressive strength.

**Citation:** Sassi, M.; Simon, A.Waste-to-Reuse Foam Glasses Produced from Soda-Lime-Silicate Glass, Cathode Ray Tube Glass, and Aluminium Dross. *Inorganics* **2022**, *10*, 1. <https://doi.org/10.3390/inorganics10010001>

Academic Editor: Rainer Niewa

Received: 30 November 2021

Accepted: 17 December 2021

Published: 21 December 2021

**Publisher's Note:** MDPI stays neutral with regard to jurisdictional claims in published maps and institutional affiliations.



**Copyright:** © 2021 by the authors. Licensee MDPI, Basel, Switzerland. This article is an open access article distributed under the terms and conditions of the Creative Commons Attribution (CC BY) license (<https://creativecommons.org/licenses/by/4.0/>).

**Keywords:** foam material; cellular materials; cathode ray tube glass; SLS glass; aluminium nitride; waste recycling

## 1. Introduction

Aluminium dross is a by-product of secondary aluminium melting when aluminium metal is produced from aluminium waste. Since as-received dross contains hazardous components, it must be treated (leached with acid or alkali followed by water washing) prior to use [1,2]. Treated aluminium dross basically contains alumina ( $\text{Al}_2\text{O}_3$ ), spinel ( $\text{MgO}\cdot\text{Al}_2\text{O}_3$ ), salt residues ( $\text{NaCl}$ ,  $\text{KCl}$ ,  $\text{CaF}_2$ ), nitride ( $\text{AlN}$ ), and small amounts of fluorides, chlorides, and other components (e.g.,  $\text{MgF}_2$ ,  $\text{NaAlCl}_4$ ,  $\text{KAlCl}_4$ ,  $\text{MgO}$ ,  $\text{KMgF}_3$ ,  $\text{SiO}_2$ ,  $\text{Fe}_2\text{O}_3$ ,  $\text{Al}_4\text{C}_3$ ,  $\text{Na}_2\text{O}$ ,  $\text{K}_2\text{NaAlF}_6$ ) [3–7]. The main problem with depositing the residual aluminium dross is the high reactivity with water and air humidity leading to the formation of hazardous and explosive gases, such as  $\text{NH}_3$ ,  $\text{CH}_4$ ,  $\text{PH}_3$ ,  $\text{H}_2$ , and  $\text{H}_2\text{S}$  [6]. Research provides several possibilities to use aluminium dross in different fields depending on the treatment method and the salt content. It served as an alumina source for the clinker burning process in the production of calcium aluminate cement with high refractory characteristics [8]. In an alkaline solution, the dross can generate hydrogen [9]. Oxide and nitride components were valorized in ceramics, glasses, and glass ceramics [7,8,10–12]. Expanded clays and foam glasses were also produced with different glass wastes and aluminium dross, where the latter acted as a foaming agent [13,14]. To date, only a few researchers have studied the foaming effect by introducing aluminium dross as a foaming agent [2].

Foam glass is a lightweight material with high load-bearing, good chemical stability, high thermal and acoustic insulating, and noninflammable properties [15]. Foam glass

typically consists of two phases, namely glass and foaming agent. When this mixture is heated above the softening point of the glass, the foaming agent releases gaseous products, which drive the expansion of the glass [16–19]. Foam glass products are used in severe working conditions such as acid or alkali corrosion environments. As it has low density, it is a favored lightweight material for in-wall insulation, filler for the restoration of failed slopes or aggregate in concrete [20–22]. The most frequent glass type is the soda-lime-silica (SLS,  $\text{Na}_2\text{O-CaO-SiO}_2$ ) glass. Millions of tons of SLS glass are produced (and become waste) worldwide in the form of container and float glass products [23]. Commercial foam glasses have 45–85 vol% porosity, 0.1–1.2  $\text{g/cm}^3$  apparent density, 0.4–6 MPa compressive strength, and 0.1–0.2 W/mK thermal conductivity [24–29]. Compressive strength is particularly important in the case of foam glass used in complex embankment applications as filling material to reduce vertical and lateral soil pressures, and to increase slope stability.

From an economical and environmental point of view, researchers use several waste materials, such as fly ash [30], cathode ray tube (CRT) glass, red mud, mineral wool waste [31,32], flat panel, and tailing waste [33] to produce building material [2,16,21,24,34–40]. The amount of CRT glass arising from computer monitors and TV sets increases dramatically due to their replacement by the liquid crystal display (LCD) [41,42]. The CRT part of monitors contains many hazardous elements (lead, strontium, antimony, barium, europium, selenium) [42–49]. The presence of lead in CRT glass makes recycling difficult and requires special safety handling. However, there are only a few CRT recycling facilities in Europe and the world [42,50]. In addition to the foam glass, CRT glass can be applied to produce a variety of building materials, such as glass-ceramic brick, geopolymer, and concrete [24,41,42,46,48,51–57].

As presented above, dross has already been applied in several cases to produce alumina, clinker, cement or glass-ceramic materials, but only a few research used dross as a foaming agent [58] or as a basic component [10] of foamed materials. In the latter case, dross is admixed only in small amounts (2.5–5–7.5 wt%) to a soda-lime glass waste [10]. This study has two special features. First, dross at increased amounts (10–20–30 wt%) is added to glass waste. Furthermore, dross and CRT glass are utilized conjointly to reveal their combined effect on the properties of the so-produced foam glass. The physical and mechanical characteristics were evaluated to establish the effect of the foam glass components on the microstructure, density, thermal conductivity, and compressive strength.

## 2. Experimental Procedures and Methods

### 2.1. Materials and Experimental Procedures

The raw materials used to produce foam glass in this work were container glass, CRT glass (provided by Daniella Ipari Park Ltd., Debrecen, Hungary), and secondary aluminium slag (produced by Arconic-Köfém Mill Products Hungary Ltd., Szekesfehervar, Hungary). The metal and salt content of the as-received dross was removed by Kekesi et al. [5] with the following method. After melting the aluminum slag to recover the molten metals, the remaining dross was crushed, milled, and washed three times with distilled water to dissolve and eliminate the salt content. Bottle and CRT glasses were milled and sieved under 70 and 32  $\mu\text{m}$  particle size, respectively. In the mixtures, SLS glass was the basic component. In addition, 5 to 10 wt% CRT glass and 10, 20, or 30 wt% dross were added to the SLS glass (Table 1). Moreover, 2 wt% silicon carbide was admixed as a foaming agent and 3 g from each mixture was poured in a stainless-steel mold then pressed under 11 MPa for 10 s into a cylindrical shape (diameter = 20 mm, height = 16 mm). Five samples from each mixture were prepared. The samples were sintered in an electric chamber furnace at different temperatures (determined through the heating microscope) with a heating rate of 5  $^\circ\text{C}/\text{min}$  and a holding time of 10 min.

**Table 1.** Composition and foaming characteristics of the mixtures.

Code	Composition, wt%			Foaming Temperature (°C)	
	Dross	SiC	CRT Glass		
BG		2		98	964
BG5CRT		2	5	93	954
BG10CRT		2	10	88	954
BG10D	10	2		88	907
BG20D	20	2		78	869
BG30D	30	2		68	880
BG5CRT10D	10	2	5	83	899
BG5CRT20D	20	2	5	73	897
BG5CRT30D	30	2	5	63	897
BG10CRT10D	10	2	10	78	922
BG10CRT20D	20	2	10	68	904
BG10CRT30D	30	2	10	58	889

## 2.2. Characterization Methods

The chemical composition of the raw materials was determined as follows:

The composition of SLS and CRT glasses was determined by an X-ray fluorescence spectrometry (XRF) instrument (Rigaku SuperMini 200). The hazardous elements in CRT glass were identified by inductively coupled plasma mass spectrometry (ICP-MS) (Varian 720 ES spectrometer). The mineral composition of the dross was analyzed by X-ray powder diffractometry (XRD) (Rigaku Miniflex II) and quantified by Rietveld-fitting.

After the process of admixing, the experimental powder mixtures were analyzed by a heating microscope (MicrOvis, Camar Elettronica) to determine the exact foaming temperature for sintering. Test samples were prepared using the pressing mold kit of the microscope. The pressed samples (with approximately 5 mm height and 2 mm diameter) are placed on an 8 × 10 mm sized alumina sheet and moved into a furnace where the sample's silhouette change in function of temperature is registered to identify the beginning of sintering, softening, sphere, half-sphere, and melting temperatures. The temperature, where the sample reached the maximum height, was identified as the foaming and sintering temperature.

After sintering in an electric chamber furnace, the samples were cut into cubic shapes where bulk density, microstructure, thermal conductivity, and compressive strength were investigated. The bulk densities of the samples were calculated as the mass per volume ( $\text{g}/\text{cm}^3$ ). The microstructure of the foams was characterized with an optic microscope (C. Zeiss Discovery V.12) by measuring the cell sizes and wall thicknesses. The cell size indicates the length (diameter) of a cell between the opposite walls. The wall thickness indicates the width of the cell wall measured perpendicularly to the edges of the wall. The statistic was made in a total of 15 measurements for each sample, where the cell size and wall thickness results were divided into six interval grades:  $d \geq 3$  mm,  $2 \text{ mm} \leq d < 3 \text{ mm}$ ,  $1 \text{ mm} \leq d < 2 \text{ mm}$ ,  $0.5 \text{ mm} \leq d < 1 \text{ mm}$ ,  $0.1 \text{ mm} \leq d < 0.5 \text{ mm}$ , and  $0.01 \text{ mm} \leq d < 0.1 \text{ mm}$  [59]. Thermal conductivity was measured by a C-Therm TCi using the Modified Transient Plane Source Method (which conforms to ASTM D7984) [60]. Compressive strength was measured using an Instron universal testing instrument on cubic shaped samples with an average cross section of 12.5 × 12 and 14 mm height. The samples were evenly loaded with a force perpendicular to their surfaces. In all of the abovementioned methods, five samples were tested.

### 3. Results and Discussion

#### 3.1. Characterization of the Raw Materials

The chemical composition of the SLS and CRT glasses is shown in Table 2. The container glass is a typical soda-lime-silica glass, which mainly consists of silica, sodium oxide, and calcium oxide with minor components, such as magnesia and alumina. CRT glass has almost the same main constituents (silica, alkali oxides, alumina) with the presence of some hazardous elements (Table 3). X-ray diffractograms of the raw materials are presented in Figure 1. Aluminium dross contains a high amount of spinel with the existence of corundum, aluminium nitride, salts, and aluminium hydroxides (Table 4). The composition of the mixtures is listed previously, in Table 1. Foam glass without any industrial waste additives is denoted as BG. CRT and D codes refer to the presence of CRT and dross, respectively. The numbers before these abbreviations show the amount (in wt%) of the components.

**Table 2.** Chemical compositions of SLS and CRT glass powder (ICP-MS analysis).

	SiO <sub>2</sub>	Na <sub>2</sub> O	K <sub>2</sub> O	CaO	MgO	Al <sub>2</sub> O <sub>3</sub>	Fe <sub>2</sub> O <sub>3</sub>	Others
SLS glass	71.5	12.5	0.72	8.75	2.44	1.75	1.15	1.19
CRT glass	55.9	5.96	5.49	0.52	0.21	1.7	0.21	30.01

**Table 3.** Hazardous elements in CRT glass (XRF analysis).

Element	Cu	Zn	Pb	Rb	As	Cr	Co	Ni	Sr	Ba	Zr
ppm	45	1891	1071	<10	53	93	<10	143	3.6	7.2	5.7

**Table 4.** Mineral composition of the dross (XRD analysis).

Formula	Phase	Wt%
MgAl <sub>2</sub> O <sub>4</sub>	Spinel	68.14
Al <sub>2</sub> O <sub>3</sub>	Corundum	17.59
AlN	Wurtzit	8.57
Al(OH) <sub>3</sub>	Bayerite	1.9
CaF <sub>2</sub>	Fluorite	1.72
NaCl	Halite	1.51
KCl	Sylvine	0.33

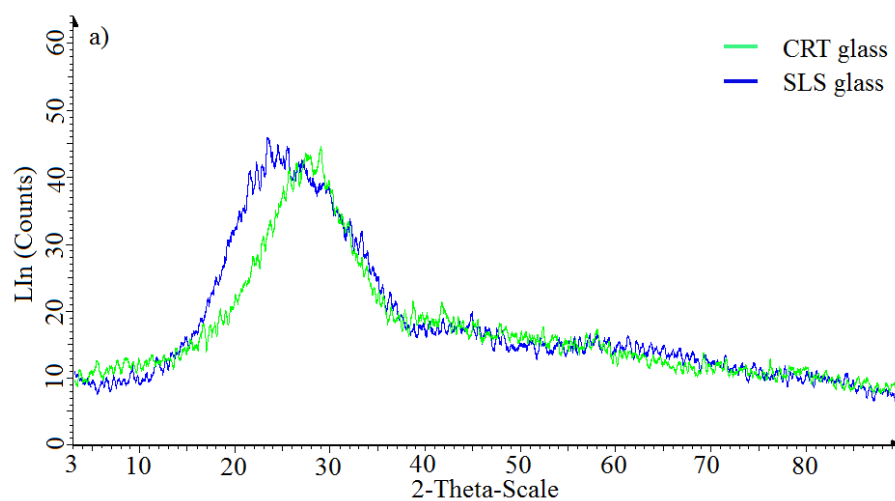


**Figure 1.** Cont.

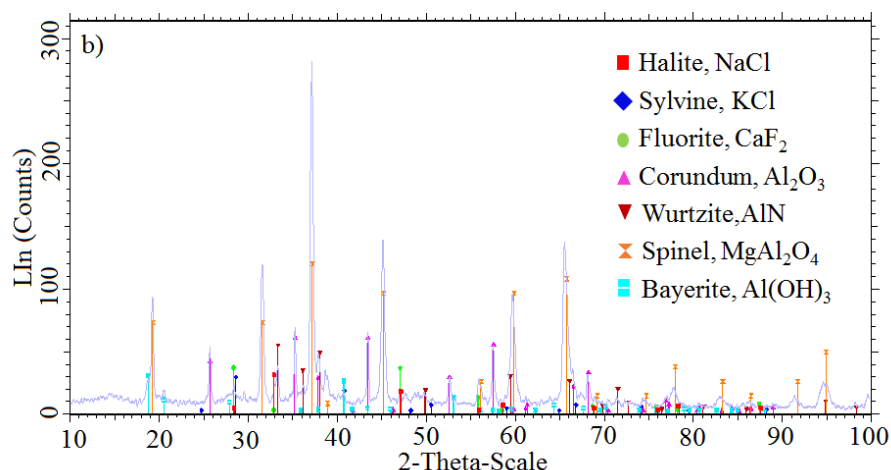
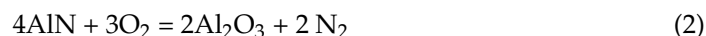
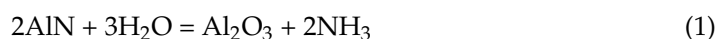


**Figure 1.** X-ray diffractograms of the raw materials. (a) SLS and CRT glass; (b) aluminum dross.

### 3.2. Sintering Behavior

To obtain the exact foaming temperature, the mixtures were analyzed by a heating microscope. The foaming temperature was determined as the temperature belonging to the maximum (foaming) height. Figures 2–4 show the sintering curves of the mixtures. Mixtures containing aluminium dross have a lower foaming temperature and higher foaming height, while dross-free mixtures show a higher foaming temperature and lower foaming height. The dross decreased the foaming temperature and enhanced the foaming process. According to Zhang et al. [2], the latter is due to the self-foaming mechanism of the dross. This foaming is based on releasing gaseous products ( $\text{NH}_3$ ,  $\text{N}_2$ , and  $\text{NO}$ ) between 800–920 °C according to the following equations:



Ewais et al. [21] found that AlN decomposed between 850–950 °C as follows:



Decreasing the foaming temperature may be due to the presence of salts (fluorite, halite, and sylvine) used in the glass industry to reduce the melting temperature of the silica glass. Sintering curves of mixtures with the SLS and CRT glasses are similar. Due to the similarity of viscosity of lead glass and commercial soda-lime-silica glass [61], adding the CRT glass by itself does not remarkably affect the foaming height, but slightly reduced the foaming temperature of the SLS glass (Figures 3 and 4) due to the lower melting point of lead glass.

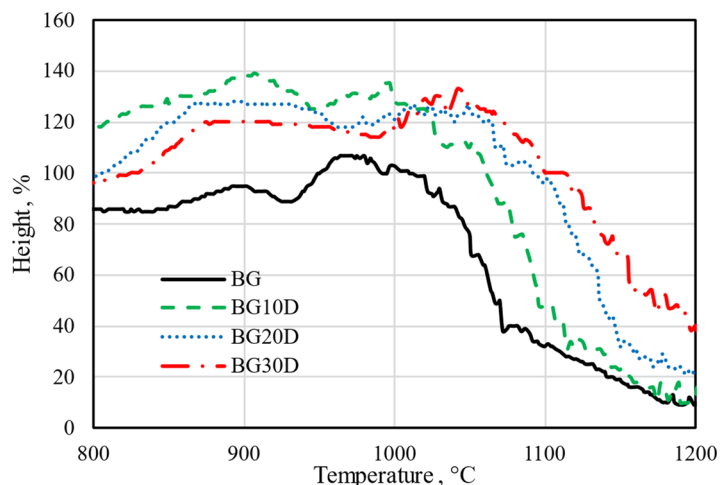


**Figure 2.** Sintering curves of glass foams with SLS glass (BG) and 10, 20, and 30 wt% dross (BG10D, BG20D, BG30D).

Mixtures with SLS glass and different amounts of dross exhibited quite similar curves (Figure 2). The addition of 20–30 wt% dross decreased the foaming temperature by 95 and 84 °C, respectively, and increased the maximum foaming height by 20 to 30%. The mixture with 10 wt% dross reached the highest foaming height (139%) and exhibited the highest foaming temperature, as well. Mixtures with 20 or 30 wt% dross content exhibited a very similar foaming behavior.

Sintering curves of mixtures with SLS glass, 5 wt% CRT glass, and different amounts of dross are represented in Figure 3. The addition of 10 wt% dross did not significantly modify the foaming temperature, but increased the maximum foaming height to 121%. Adding 20 wt% dross attained a 20% increase in the maximum foaming height. In addition, 30 wt% dross resulted in the same foaming height as 10 wt%. In this series, a mixture with 20 wt% dross contents represented the best combination of maximum foaming height and temperature. Contrary to the previous series, adding the highest amount of CRT glass (10 wt%) increased the foaming height to 136%. By increasing the dross content, the maximum foaming height may reach 148% with 20 wt% dross.

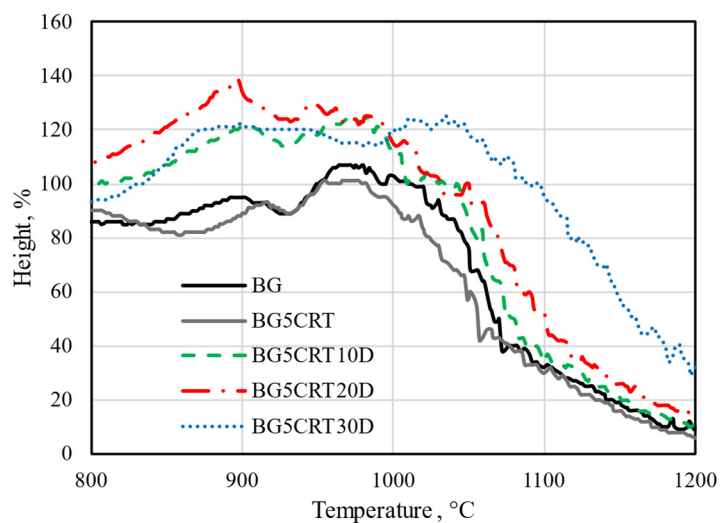


**Figure 3.** Sintering curves of glass foams with SLS glass (BG), 5 wt% CRT and 10, 20, and 30 wt% dross (BG5CRT10D, BG5CRT20D, BG5CRT30D).

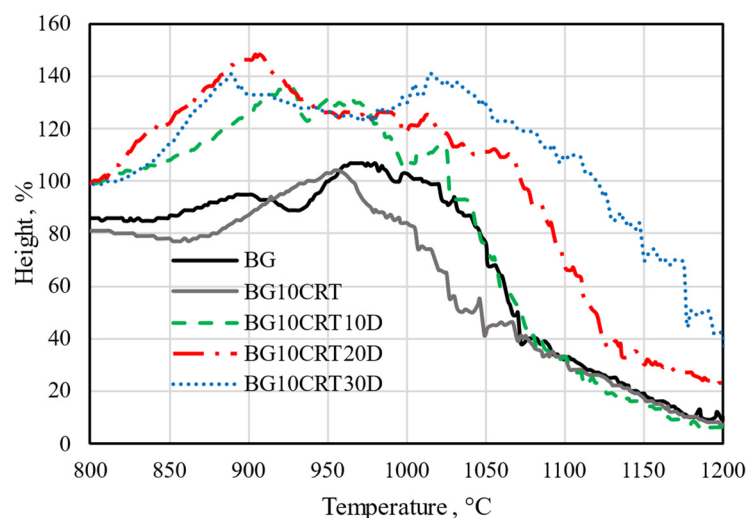


**Figure 4.** Sintering curves of glass foams with SLS glass (BG), 10 wt% CRT and 10, 20, and 30 wt% dross (BG10CRT10D, BG10CRT20D, BG10CRT30D).

Oxides forming the glass are categorized into three groups: Network forming, modifier, and intermediate. Network forming oxides (e.g.,  $\text{SiO}_2$ ) build the basic units (silica tetrahedron) of the glass structure. The modifiers change this structure—by sitting in the voids of the network, they can change the angle and the position of the bonds or even break them. Intermediate oxides functionate as network forming and modifiers, as well. Dross contains both modifier ( $\text{MgO}$ ) and intermediate ( $\text{Al}_2\text{O}_3$ ) oxides. When dross is added to the silica (SLS) glass, the  $\equiv\text{Si-O-Si}\equiv$  bonds are replaced by  $\equiv\text{Si-O-Mg-O-Si}\equiv$  bonds or aluminates tetrahedra are formed rather than the silicate tetrahedra. Additionally,  $\text{Al}_2\text{O}_3$  increases the melting point of the glass. On the contrary,  $\text{PbO}$ ,  $\text{BaO}$ , and  $\text{SrO}$  (components of CRT glass) decrease the melting point of the mixture.  $\text{PbO}$  also works as an intermediate oxide, which means it can be integrated into the glass network. By increasing the CRT glass content, additional silicate tetrahedra are replaced by Pb-based units. However, as Pb atoms and ions have larger atomic or ionic radii with a smaller charge, the formed Pb-O bonds are weaker than the Si-O bonds. Ben Kacem et al. [62] studied the structure and properties of lead silicate glasses and melts using Roman spectra. The glass transition temperature and viscosity measurements exhibit a strong decrease with the increasing  $\text{PbO}$  content. This aspect is correlated with the network depolymerization of the silicate network with the creation of non-bridging oxygens replacing bridging oxygens observed by Raman spectroscopy. Moreover, the difference of adding  $\text{Na}_2\text{O}$  and  $\text{PbO}$  on the glass transition temperature ( $T_g$ ) becomes smaller when the content of the network modifier is getting higher and the effect on the glass transition temperature becomes closer. This might be the reason to lower the foaming temperature in the samples containing CRT glass and dross and to create a favorable viscosity allowing gas bubbles generation, consequently, increasing the foaming height in comparison with the base silicate foam glass. Based on the literature review, the decomposition of  $\text{AlN}$  takes place at 800–950 °C [2,23]. This range is mostly covered by samples with CRT glass and dross at the same time. A combination of lower softening (melting) temperatures and enhanced decomposition of  $\text{AlN}$  in the dross leads to lowering the foaming temperature and boosting the foaming process.

### 3.3. Microstructure

The microstructural analysis of the foam glasses was conducted on the cubic shaped samples. It shows a diversified picture (Figure 5). Dross-free samples had thin cell walls with medium average cell size (1.11–1.4 mm). The shape of the pores ranges from round through oval to irregular polygons. Both open and closed pores were formed in the structure. By adding 10 wt% of dross, the ratio of larger pores increased while the shape of the pores was still diversified. Round-shaped pores indicate they were formed in a viscous

environment [24], while oval or irregular-shaped pores refer to a boosted foaming process resulting in their growth and coalescence [2]. The densest microstructures with irregularly shaped pores were observed in foams with 30 wt% dross. According to Veit and Rüssel [63], substituting  $\text{SiO}_2$  by  $\text{Al}_2\text{O}_3$  in the glass network does not cause significant changes in the viscosity, but replacing  $\text{CaO}$  with  $\text{MgO}$  increases the viscosity. On the contrary, Zhang et al. found [2] that the increase in  $\text{Al}_2\text{O}_3$  content leads to a slight increase in the softening temperature and decelerates the liquid phase formation.

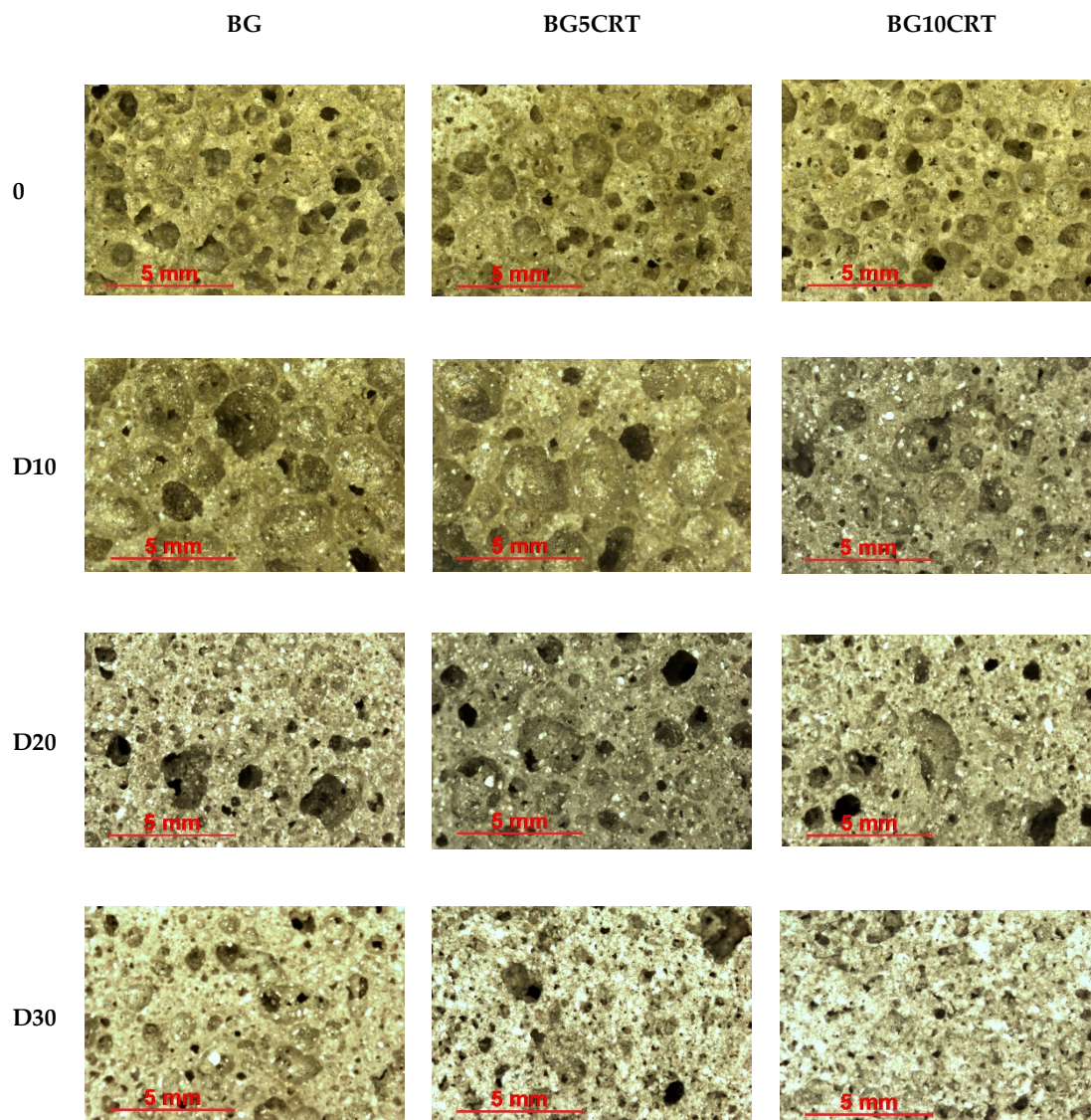


**Figure 5.** Microstructure of the foam glasses (scale bar = 5 mm).

As larger pores weaken the structure and may cause defects during the lifetime of products [2], the maximum cell sizes were determined in addition to the average cell size and wall thickness (Figures 6 and 7). Both the average and maximum cell size reached the highest value at 10 wt% dross contents independently from the CRT content. By increasing the dross content to 30 wt%, the cell sizes became even smaller than in the dross-free foams. A similar behavior was observed by Zhang et al. [2]. The average cell size, maximum cell size, and average wall thickness of the foamed samples ranged between 0.5–2.3 mm, 0.9–2.9 mm, and 0.3–1.2 mm, respectively.

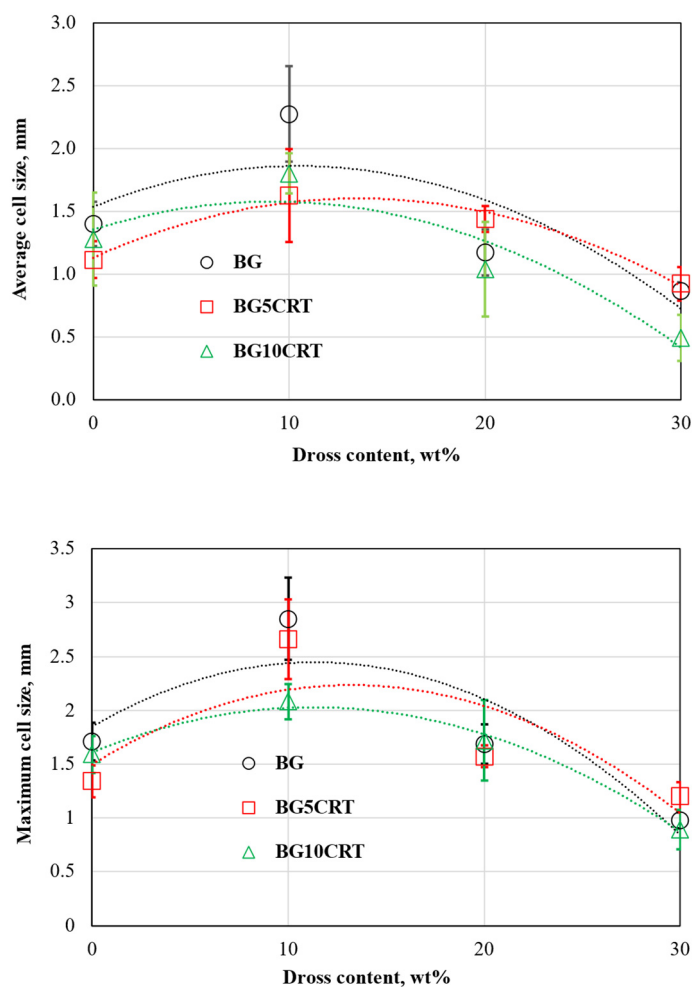


**Figure 6.** Average and maximum cell sizes of the foam glasses.

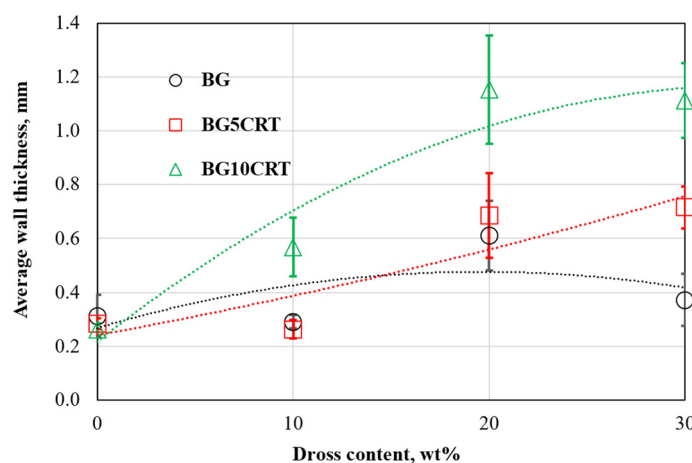


**Figure 7.** Average wall thickness of the foam glasses.

### 3.4. Properties

Figure 8 shows the density of the sintered foams in the function of dross content. The density of the sintered foams ranges between 0.23–0.92 g/cm<sup>3</sup>, which fulfills the requirements of commercial foam glasses. Increasing the dross content increased the density in general. It is following the microstructural observations, where the densest structure belonged to the 30 wt% dross contents. It has presumably two reasons. Adding

PbO, BaO, SrO (originating from the CRT glass), and MgO, Al<sub>2</sub>O<sub>3</sub> (originating from the dross) to the pristine SLS glass increased the density of the glass phase. In addition, the presence of MgO and Al<sub>2</sub>O<sub>3</sub> in the glass structure increased the viscosity and lessened the liquid phase during sintering. As the ratio of the liquid phase decreases and the viscosity increases, the formation of bubbles becomes more hindered.

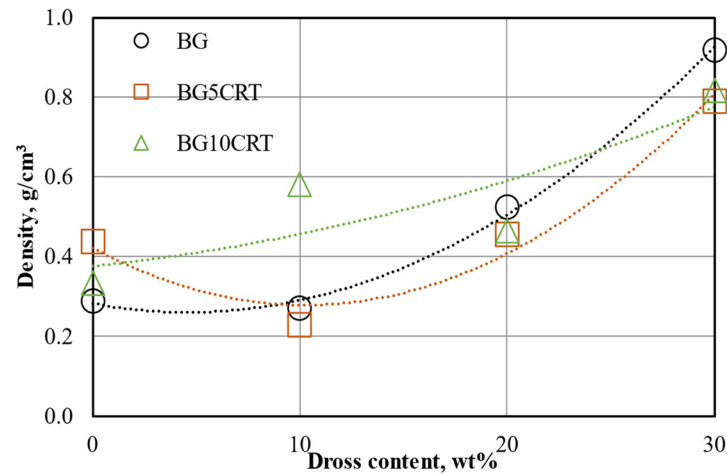


**Figure 8.** Bulk density of the samples of foam glasses.

Thermal conductivity curves are plotted in Figure 9. The thermal conductivity coefficient ranged from 0.037 to 0.068 W/mK representing a good insulation efficiency. The density, cell size, and wall thickness have a direct influence on the thermal conductivity. In general, thermal conductivity follows the same trend as the density, while the cell size curves are opposite to the thermal conductivity. Heat flow is propagated through the cell walls. The thickness of the wall affects the heat conduction, the thicker the wall the higher the conduction. Thermal insulation can be enhanced in the case of homogenous microstructure and better arrangement of the cells [59]. Thermal conductivity depends on the size of the cells, the bigger the cells the better the thermal insulation. Another important factor that affects the thermal conductivity is the uniformity (homogeneity) of the cells. The heterogeneous cell size in a sample gives better thermal insulation.

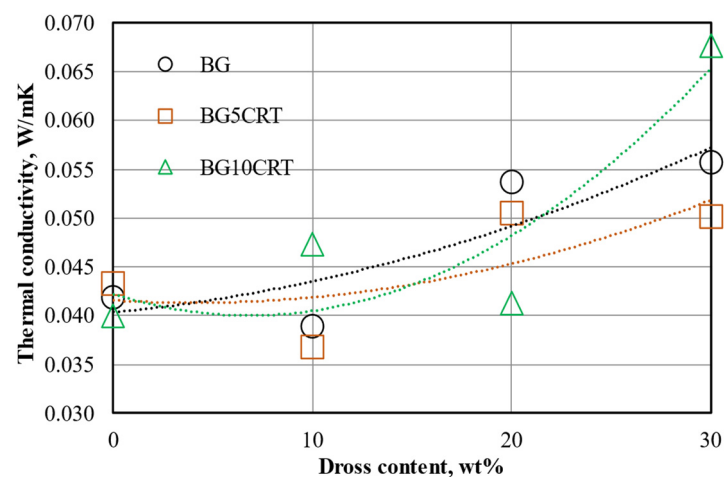


**Figure 9.** Thermal conductivity of foam glasses.

The compressive strength (Figure 10) of the sintered foams ranges between 0.7–5.7 MPa. Adding dross to the SLS glass decreased the strength from 2.5 to 0.9 MPa. The CRT glass content increased the compressive strength. Foams with CRT glass and 30 wt% dross exhibited a denser microstructure and thicker walls, which provide better load-bearing

properties and give better strength. In samples with a small dross content, large pores were formed during sintering resulting in lower density and lower strength.

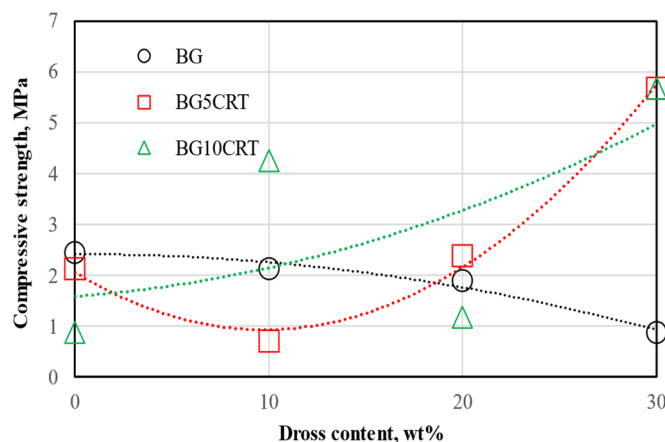


Figure 10. Compressive strength of foam glasses.

#### 4. Conclusions

Foam glasses were successfully made from the SLS glass material, cathode ray tube (CRT) glass (5 and 10 wt%), treated secondary aluminium dross (10, 20, and 30 wt%), and silicon carbide (2 wt%). The effect of the foam glass composition on the microstructure, density, thermal conductivity, and compressive strength was characterized. Aluminium dross acted as a foaming agent and a component enhancing the compressive strength of the foam glasses at the same time.

Adding aluminium dross decreased the foaming temperature and increased the foaming height. The former may be due to the presence of salts (fluorite, halite, and sylvine), which are used in the glass industry to reduce the melting temperature of the silica glass. The foaming process is enhanced due to the changes in intramolecular bonds and viscosity. When dross is added to the silica (SLS) glass, the  $\equiv\text{Si-O-Si}\equiv$  bonds are replaced by  $\equiv\text{Si-O-Mg-O-Si}\equiv$  bonds or aluminate tetrahedra are formed rather than the silicate tetrahedra. Additionally, the components of the dross ( $\text{MgO}$ ,  $\text{Al}_2\text{O}_3$ ) play the role of a modifier and intermediate oxide, respectively. Furthermore,  $\text{Al}_2\text{O}_3$  increases the melting point of the glass. On the contrary,  $\text{PbO}$ ,  $\text{BaO}$ , and  $\text{SrO}$  (components of the CRT glass) decrease the melting point of the mixture.

The microstructure of the foam glasses was affected by the initial composition and the added amount of aluminium dross. The shape of the pores ranges from round through oval to irregular polygons. Both open and closed pores are formed in the structure. The densest microstructures with irregularly shaped pores are observed in foams with 30 wt% dross.

The microstructure of the foam glass influenced the thermal conductivity and compressive strength of the samples. Thermal conductivity depends on the size of the cells, the bigger the cells, the better the thermal insulation. The heterogeneous cell size distribution gives better thermal insulation. Samples with smaller pores and higher dross content have the highest compressive strength.

**Author Contributions:** Conceptualization, M.S. and A.S.; methodology, M.S. and A.S.; software, M.S.; validation M.S. and A.S.; formal analysis, M.S.; investigation, M.S.; resources, A.S.; data curation, M.S.; writing—original draft preparation, M.S. and A.S.; writing—review and editing M.S. and A.S.; visualization, M.S.; supervision, A.S.; project administration, A.S.; funding acquisition, A.S. All authors have read and agreed to the published version of the manuscript.

**Funding:** The research work was supported by the GINOP2.2.1-15-2016-00018 project in the framework of the New Széchenyi Plan of Hungary, co-financed by the European Social Fund, aimed to enhance the R&D&I activities between the joined Hungarian universities and the Arconic-Köfém Mill Products Hungary Ltd.

**Institutional Review Board Statement:** Not applicable.

**Informed Consent Statement:** Not applicable.

**Data Availability Statement:** The data that support the findings and conclusions of this study are available from the corresponding author upon reasonable request.

**Acknowledgments:** The authors take the opportunity to welcome the support of Daniella Ipari Park Ltd., and Arconic-Köfém Mill Products Hungary Ltd. for their support. The contribution of Tamas Kekesi, Karoly Gal, Istvan Kocserha, Oliver Banhidi, Ferencz Móricz, and Ildiko Tasnadi in the pretreatment of the dross, heating microscopy, XRD, ICP-MS, XRF, and compressive strength tests, respectively, is greatly appreciated.

**Conflicts of Interest:** The authors declare no conflict of interest.

## References

1. Shen, H.; Liu, B.; Ekberg, C.; Zhang, S. Harmless disposal and resource utilization for secondary aluminum dross: A review. *Sci. Total Environ.* **2021**, *760*, 143968. [CrossRef]
2. Zhang, J.; Liu, B.; Zhao, S.; Shen, H.; Liu, J.; Zhang, S. Preparation and characterization of glass ceramic foams based on municipal solid waste incineration ashes using secondary aluminium ash as foaming agent. *Constr. Build. Mater.* **2020**, *262*, 120781. [CrossRef]
3. Hwang, J.; Huang, X.; Xu, Z. Recovery of Metals from Aluminum Dross and Saltcake. *J. Miner. Mater. Charact. Eng.* **2006**, *5*, 47–62. [CrossRef]
4. Kekesi, T. Characterization and complete utilization of aluminium melting dross. In Proceedings of the International V4 Waste Recycling 21 Conference, Miskolc, Miskolci Egyetem, Miskolc-Egyetemváros, Hungary, 22–23 November 2018; pp. 162–177, ISBN 9789633581735.
5. Illés, I.; Sassi, M.; Zakiyya, H.; Kékesi, T. The Fundamental Kinetic Characteristics of Aqueous Dissolution of Chloride and Fluoride Salts from Secondary Aluminium Dross. Kékesi, Tamás (szerk.) MultiScience—XXXIII. In Proceedings of the microCAD International Multidisciplinary Scientific Conference 2019, Miskolc, Hungary, 23 May 2017.
6. Mostafa, M.; Ali, A. Enhanced alumina recovery from secondary aluminum dross for high purity nanostructured alumina powder production: Kinetic study. *J. Environ. Manag.* **2018**, *212*, 278–291.
7. Theam, Y.; Ee, L.; Mohd, F.; Shahabaldin, R. Optimization of aluminium recovery from water treatment sludge using response surface methodology. *J. Environ. Manag.* **2018**, *228*, 13–19.
8. Tsakiridis, P. Aluminium salt slag characterization and utilization. *J. Hazard. Mater.* **2012**, *217–218*, 1–10. [CrossRef]
9. Elsarrag, E.; Elhoweris, A.; Alhorri, Y. The production of hydrogen as an alternative energy carrier from aluminium waste. *Energy Sustain. Soc.* **2017**, *7*, 9. [CrossRef]
10. El-Amir, A.A.; Attia, M.A.; Newishy, M.; Fend, T.; Emad, M. Aluminium dross/soda lime glass waste-derived high-quality glass foam. *J. Mater. Res. Technol.* **2021**, *15*, 4940–4948. [CrossRef]
11. Sassi, M.; Ibrahim, J.-E.F.M.; Simon, A. Characterization of foam glass produced from waste CRT glass and aluminium dross. *J. Phys. Conf. Ser.* **2020**, *1527*, 012037. [CrossRef]
12. Tsakiridis, P.; Oustadakis, P.; Agatzini-Leonardou, S. Aluminium recovery during black dross hydrothermal treatment. *J. Environ. Chem. Eng.* **2013**, *1*, 23–32. [CrossRef]
13. Bajare, D.; Korjakins, A.; Kazjonovs, J. Application of aluminium dross and glass waste for production of expanded clay aggregate. In Proceedings of the 3rd International Scientific Conference, Riga, Latvia, 13 October 2011.
14. Arunabh, M.; Kamalesh, K. Recovery of valuable products from hazardous aluminum dross: A review. *Resour. Conserv. Recycl.* **2018**, *130*, 95–108.
15. Bozsaky, D. The historical development of thermal insulation materials. *Period. Polytech. Archit.* **2010**, *41*, 49–56. [CrossRef]
16. Attila, Y.; Guden, M.; Tasdemirci, A. Foam glass processing using a polishing glass powder residue. *Ceram. Int.* **2013**, *39*, 5869–5877. [CrossRef]
17. Marinov, M.; Lakov, L.T. Granulated foam glass. Production, physical and mechanical properties. *Sci. Proceeding XIII Int. Congr. Mach. Technol. Mater.* **2016**, *10*, 42–44.
18. Taoyong, L.; Piao, L.; Xiaogang, G.; Jiashuo, Z.; Qianxing, H.; Zhiwei, L.; Zhou, X.; Qifeng, Y.; Yougen, T.; Anxian, L. Preparation, characterization and discussion of glass ceramic foam material: Analysis of glass phase, fractal dimension and self-foaming mechanism. *Mater. Chem. Phys.* **2020**, *243*, 122614.
19. Li, J.; Zhuang, X.; Monfort, E.; Querol, X.; Llaudis, A.S.; Font, O.; Moreno, N.; Ten, F.J.G.; Maria, I. Utilization of coal fly ash from a Chinese power plant for manufacturing highly insulating foam glass: Implications of physical, mechanical properties and environmental features. *Constr. Build. Mater.* **2018**, *175*, 64–76. [CrossRef]
20. Foamit, Foamit, Applications for Civil Engineering. 2019. Available online: <http://www.foamit.fi/wp-content/uploads/2016/10/Foamedglass.pdf> (accessed on 1 November 2021).
21. Baidzhanov, D.; Nuguzhinov, Z.S.; Fedorchenko, V.; Kropachev, P.A. Thermal insulation material based on local technogenic raw material. *Glass Ceram.* **2016**, *73*, 427–430. [CrossRef]

22. Hu, L.; Bu, F.; Guo, F.; Zhang, Z. Construction method of foam glass thermal insulation material in sloping roof. *IOP Conf. Ser. Earth Environ. Sci.* **2017**, *61*, 012122. [[CrossRef](#)]
23. Ewais, E.M.M.; Attia, M.A.; El-Amir, A.A.; Elshenway, A.M.; Fend, T. Optimal conditions and significant factors for fabrication of soda lime glass foam from industrial waste using nano AlN. *J. Alloys Compd.* **2018**, *747*, 408–415. [[CrossRef](#)]
24. Barbosa, A.R.J.; Lopes, A.A.S.; Sequeira, S.I.H.; Oliveira, J.P.; Davarpanah, A.; Mohseni, F.; Amaral, V.S.; Monteiro, R.C.C. Effect of processing conditions on the properties of recycled cathode ray tube glass foams. *J. Porous Mater.* **2016**, *23*, 1663–1669. [[CrossRef](#)]
25. König, J.; Lopez-Gil, A.; Cimavilla-Roman, P.; Rodriguez-Perez, M.A.; Petersen, R.R.; Østergaard, M.B.; Iversen, N.; Yue, Y.; Matjaž, S. Synthesis and properties of open- and closed-porous foamed glass with a low density. *Constr. Build. Mater.* **2020**, *247*, 118574. [[CrossRef](#)]
26. König, J.; Nemanic, V.; Zumer, M.; Rasmus, R.P.; Martin, B.Ø.; Yue, Y.; Suvorov, D. Evaluation of the contributions to the effective thermal conductivity of an open-porous-type foamed glass. *Constr. Build. Mater.* **2019**, *214*, 337–343. [[CrossRef](#)]
27. da Silva, R.C.; Kubaski, E.T.; Tenório-Neto, E.T.; Lima-Tenório, M.K.; Tebcherani, S.M. Foam glass using sodium hydroxide as foaming agent: Study on the reaction mechanism in soda-lime glass matrix. *J. Non-Cryst. Solids* **2019**, *511*, 177–182. [[CrossRef](#)]
28. Bai, C.; Li, H.; Bernardo, E.; Colombo, P. Waste-to-resource preparation of glass-containing foams from geopolymers. *Ceram. Int.* **2018**, *45*, 7196–7202. [[CrossRef](#)]
29. Arriagada, C.; Navarrete, I.; Lopez, M. Understanding the effect of porosity on the mechanical and thermal performance of glass foam lightweight aggregates and the influence of production factors. *Constr. Build. Mater.* **2019**, *228*, 116746. [[CrossRef](#)]
30. Wang, H.; Chen, Z.; Ji, R.; Liu, L.; Wang, X. Integrated utilization of high alumina fly ash for synthesis of foam glass ceramic. *Ceram. Int.* **2018**, *44*, 13681–13688. [[CrossRef](#)]
31. Ji, R.; Zheng, Y.; Zou, Z.; Chen, Z.; Wei, S.; Jin, X.; Zhang, M. Utilization of mineral wool waste and waste glass for synthesis of foam glass at low temperature. *Constr. Build. Mater.* **2019**, *215*, 623–632. [[CrossRef](#)]
32. Chen, Z.; Wang, H.; Ji, R.; Liu, L.; Cheeseman, C.; Wang, X. Reuse of mineral wool waste and recycled glass in ceramic foams. *Ceram. Int.* **2019**, *45*, 15057–15064. [[CrossRef](#)]
33. Taoyong, L.; Changwei, L.; Jianlei, L.; Lei, H.; Hua, G.; Cui, L.; Xin, Z.; Hui, T.; Qifeng, Y.; Anxian, L. Phase evolution, pore morphology and microstructure of glass ceramic foams derived from tailings wastes. *Ceram. Int.* **2018**, *44*, 14393–14400.
34. Nagrockiene, D.; Barkauskas, K. Utilization of Waste Glass Powder in Cement Mortar. *Environ. Sci. Proc.* **2021**, *9*, 25. [[CrossRef](#)]
35. Kurpinska, M.; Leszek, K.; Miruszewski, T.; Byczuk, M. Application of artificial neural networks to predict insulation properties of lightweight concrete. *Appl. Sci.* **2021**, *11*, 10544. [[CrossRef](#)]
36. Yuxi, G.; Yihe, Z.; Hongwei, H.; Ke, M.; Kunran, H.; Pan, H.; Wang, X.; Zhilei, Z.; Xianghai, M. Novel glass ceramic foams materials based on red mud. *Ceram. Int.* **2014**, *40*, 6677–6683.
37. Tulyaganov, D.; Fernandes, H.; Agathopoulos, S.; Ferreira, J. Preparation and characterization of high compressive strength foams from sheet glass. *J. Porous Mater.* **2006**, *13*, 33–139. [[CrossRef](#)]
38. Yang, L.; Shili, Z.; Shuhua, M.; Chunli, L.; Xiaohui, W. Preparation of sintered foamed ceramics derived entirely from coal fly ash. *Constr. Build. Mater.* **2018**, *163*, 529–538.
39. Xi, C.; Zheng, F.; Jiahe, X.; Yang, W.; Peng, Y.; Li, Y.; Li, P.; Zhen, Q. Preparation of glass-ceramic foams using extracted titanium tailing and glass waste as raw materials. *Constr. Build. Mater.* **2018**, *190*, 896–909. [[CrossRef](#)]
40. Bawab, J.; Khatib, J.; Jahami, A.; Elkordi, A.; Ghorbel, E. Structural performance of reinforced concrete beams incorporating Cathode-Ray Tube (CRT) glass Waste. *Buildings* **2021**, *11*, 67. [[CrossRef](#)]
41. Choi, S.Y.; Choi, Y.S.; Kim, I.S.; Yang, E.I. An Experimental Study on Flexural Behaviors of Reinforced Concrete Member Replaced Heavyweight Waste Glass as Fine Aggregate under Cyclic Loading. *Appl. Sci.* **2018**, *8*, 2208. [[CrossRef](#)]
42. Meng, W.; Wang, X.; Yuan, W.; Wang, J.; Songa, G. The recycling of leaded glass in cathode ray tube (CRT). *Procedia Environ. Sci.* **2016**, *31*, 954–960. [[CrossRef](#)]
43. Grause, G.; Takahashi, K.; Yoshioka, T. Thermogravimetric Investigation of the Lead Volatilization from Waste Cathode-Ray Tube Glass. *Recycling* **2016**, *1*, 111–121. [[CrossRef](#)]
44. Imre-Lucaci, A.; Fogarasi, M.; Imre-Lucaci, F.; Fogarasi, S. Chemical–electrochemical process concept for lead recovery from waste Cathode Ray Tube glass. *Materials* **2021**, *14*, 1546. [[CrossRef](#)]
45. Catauro, M.; Lancellotti, I.; Leonelli, C. Addition of WEEE glass to metakaolin-based geopolymeric Binder: A cytotoxicity study. *Environments* **2017**, *4*, 89. [[CrossRef](#)]
46. Bernardo, E.; Scarinci, G.; Hreglich, S.; Zangiacomì, G. Effect of time and furnace atmosphere on the sintering of glasses from dismantled cathode ray tubes. *J. Eur. Ceram. Soc.* **2007**, *27*, 1637–1643. [[CrossRef](#)]
47. Bertoncetto, R.; Milanese, L.; Bouquillon, A.; Dran, J.; Mille, B.; Salomon, J. Leaching of lead silicate glasses in acid environment: Compositional and structural changes. *Appl. Phys* **2004**, *79*, 193–198. [[CrossRef](#)]
48. Østergaard, M.B.; Petersen, R.R.; König, J.; Yue, Y. Effect of alkali phosphate content on foaming of CRT panel glass using Mn<sub>3</sub>O<sub>4</sub> and carbon as foaming agents. *J. Non-Cryst. Solids* **2017**, *482*, 217–222. [[CrossRef](#)]
49. Méar, F.; Yot, P.; Cambon, M.; Ribes, M. The characterization of waste cathode-ray tube glass. *Waste Manag.* **2016**, *26*, 1468–1476. [[CrossRef](#)]
50. Ledwaba, P.; Sosibo, N. Cathode Ray Tube Recycling in South Africa. *Recycling* **2017**, *2*, 4. [[CrossRef](#)]
51. Górski, M.; Wielgus, N.; Loska, K.; Koziół, M.; Landrat, M.; Scierski, W.; Pikon, K. Characteristics of metakaolin-based geopolymer with Cathode Ray Tube glass. *Polymers* **2021**, *13*, 1149. [[CrossRef](#)]

52. Bawab, J.; Khatib, J.; El-Hassan, H.; Assi, L.; Kırgız, M.S. Properties of cement-based Materials Containing Cathode-Ray Tube (CRT) glass waste as fine aggregates—A Review. *Sustainability* **2021**, *13*, 11529. [[CrossRef](#)]
53. Wielgus, N.; Górski, M.; Kubica, J. Discarded Cathode Ray Tube glass as an alternative for aggregate in a metakaolin-based geopolymer. *Sustainability* **2021**, *13*, 479. [[CrossRef](#)]
54. Grdic, D.Z.; Toplicic-Curcic, G.A.; Grdic, Z.J.; Risti, N.S. Durability Properties of Concrete Supplemented with Recycled CRT Glass as Cementitious Material. *Materials* **2021**, *14*, 4421. [[CrossRef](#)]
55. Cabrera, M.; Pérez, P.; Rosales, J.; Agrela, F. Feasible use of Cathode Ray Tube glass (CRT) and Recycled Aggregates as Unbound and Cement-Treated granular Materials for Road Sub-Bases. *Materials* **2020**, *13*, 748. [[CrossRef](#)] [[PubMed](#)]
56. Mucsi, G.; CsYke, B.; Kertész, M.; Hoffmann, L. Physical Characteristics and Technology of Glass Foam from Waste Cathode Ray Tube Glass. *J. Mater.* **2013**, *2013*, 696428. [[CrossRef](#)]
57. Cosmin, V.; Lazău, I. Glass foam from window panes and bottle glass wastes. *Cent. Eur. J. Chem.* **2014**, *12*, 804–811.
58. Shi, H.; Feng, K.; Wang, H.; Chen, C.; Zhou, H. Influence of aluminium nitride as a foaming agent on the preparation of foam. *Int. J. Miner. Metall. Mater.* **2016**, *23*, 595. [[CrossRef](#)]
59. Qin, Z.; Li, G.; Tian, Y.; Ma, Y.; Shen, P. Numerical Simulation of Thermal Conductivity of Foam Glass Based on the Steady-State Method. *Materials* **2018**, *12*, 54. [[CrossRef](#)]
60. C-THERM TCi. Available online: [https://ctherm.com/products/tci\\_thermal\\_conductivity/how\\_the\\_tci\\_works/mtps/](https://ctherm.com/products/tci_thermal_conductivity/how_the_tci_works/mtps/) (accessed on 1 November 2021).
61. Glass Viscosity Calculation. Available online: <https://glassproperties.com/viscosity/> (accessed on 1 November 2021).
62. Kacem, I.B.; Gautron, L.; Coillot, D.; Neuville, D.R. Structure and properties of lead silicate glasses and melts. *Chem. Geol.* **2017**, *461*, 104–114. [[CrossRef](#)]
63. Veit, U.; Rüssel, C. Viscosity and liquidus temperature of quaternary glasses close to an eutectic composition in the CaO–MgO–Al<sub>2</sub>O<sub>3</sub>–SiO<sub>2</sub> system. *J. Mater. Sci.* **2017**, *52*, 8280–8292. [[CrossRef](#)]